Available online at www.sciencedirect.com
ScienceDirect
Journal of Sound and Vibration 312 (2008) 713–725
JOURNAL OF SOUND AND VIBRATION
www.elsevier.com/locate/jsvi

Free vibration of a cantilevered beam with multiple steps: Comparison of several theoretical methods with experiment

J.W. Jaworski*, E.H. Dowell

Department of Mechanical Engineering and Materials Science, Duke University, Durham, NC 27708, USA

Received 8 August 2006; received in revised form 5 November 2007; accepted 7 November 2007
Available online 20 February 2008

Abstract

The flexural-free vibration of a cantilevered beam with multiple cross-section steps is investigated theoretically and experimentally. Experimental results are compared against Euler–Bernoulli beam theory solutions from Rayleigh–Ritz and component modal analyses, as well as finite element results using the commercial package ANSYS. Finite elements are also used to investigate a Timoshenko beam, a two-dimensional shell, and a three-dimensional solid element model. A detectable difference in the first in-plane bending natural frequency is noted between the beam theory results and those of the higher-dimensional finite element models and experimental observation. The convergence of the several theoretical approaches and their effectiveness as analysis and design methods for multiple-stepped beams are also discussed.

1. Introduction

The present work considers the accuracy and convergence of the classic Rayleigh–Ritz method, component modal analysis, and the finite element method as applied to the free vibration analysis of a multiple-stepped cantilevered beam. Existing work on stepped beams relies heavily on Euler–Bernoulli and Timoshenko beam theories for both approximate and exact solutions, which are seldom compared with experiment. Using standard methods, the present investigation addresses the impact of inter-component boundary conditions, method convergence, and model fidelity on the accuracy of free vibration results for multiple-stepped beams. A brief review of prior research on stepped beams follows.

Early research by Taleb and Suppiger [1] used the single-stepped beam on simple supports as a test case for approximate free vibration solutions using the Cauchy iteration method, which provided upper-bound frequency results. Buckens [2] employed the decomposition method to establish a useful lower bound for the same stepped beam problem as well as a multiple-stepped beam. Klein [3] adapted a variational component approach with Lagrange multipliers to explicitly enforce geometric continuity between components; this method is among those employed in the present work. Yuan and Dickinson [4] incorporated artificial spring constraints between beam components into the Rayleigh–Ritz energy approach, which yielded accurate fundamental frequency results. Maurizi and Bellés extended the artificial spring concept to the global

*Corresponding author. Tel.: +1 919 660 5055; Fax: +1 919 660 0089.
E-mail addresses: jwj@duke.edu (J.W. Jaworski), dowell@ee.duke.edu (E.H. Dowell).

0022-460X/$ - see front matter © 2007 Elsevier Ltd. All rights reserved.
doi:10.1016/j.jsv.2007.11.010

boundary conditions, including cantilever [5] and other classical support scenarios [6]. Lee and Ng [7] used the step thickness ratio to compare the suitability of the artificial spring and standard global Rayleigh–Ritz methods. Popplewell and Chang [8] used the so-called "force mode functions" to improve the global Rayleigh–Ritz method convergence by introducing discontinuities into the second and third derivatives of the assumed deflection.

The exact solution by Levinson [9] of the single-stepped beam on simple supports led to further "exact" method investigations for more complicated arrangements. Jang and Bert [10,11] tabulated results for a single, centrally stepped beam on classical supports using a determinant form of the continuity equations in terms of the global boundary conditions. Naguleswaran extended this approach to a wide variety of system parameters [12] and to three step-changes in cross-section [13]. The beneficial effect of dynamic stiffening via judicious material removal for cantilevered beams was reported and discussed by Subramanian and Balasubramanian [14] and validated experimentally by Laura et al. [15].

The examples provided in the works referenced above address only the single, centrally stepped beam with Euler–Bernoulli beam physics. Gorman [16] tabulated exact solutions for different step-discontinuity locations and for beams with symmetric discontinuities and end supports. The recent work of Koplow et al. [17] analyzes exactly the dynamic response of a beam with an asymmetric step discontinuity and aligned neutral axis, including comparisons with a receptance coupling method and experiment. Ju et al. [18] investigated the implications of shear deformation and step eccentricity for a beam with two steps down using first-order shear deformation Timoshenko beam theory, noting only a "slight change" in cantilever modal results due to step eccentricity. Farghaly and Elmahdy [19] reported good agreement between Timoshenko theory predictions and experiment for beams with several steps down. To the authors' knowledge, no experimental data exists in the literature for a cantilevered beam that is both stepped down *and* stepped up.

2. Analysis

2.1. Rayleigh–Ritz method

The kinetic and strain energies per unit span due to flexural bending are defined, respectively, as

$$\frac{T}{L}=\frac{1}{2}\int_0^1 m(x)\left(\frac{\partial w}{\partial t}\right)^2 \mathrm{d}x, \tag{1}$$

$$\frac{V}{L}=\frac{1}{2}\int_0^1 \frac{EI(x)}{L^4}\left(\frac{\partial^2 w}{\partial x^2}\right)^2 \mathrm{d}x. \tag{2}$$

The transverse beam deflection is an assumed series solution:

$$w(x,t)=\sum_n q_n(t)W_n(x). \tag{3}$$

The spanwise variable x is scaled by the total beam length L. The mass per unit length is $m(x)$, and $EI(x)$ denotes the flexural rigidity as a function of span. Also, $q_n(t)$ and $W_n(x)$ are the nth generalized coordinate and assumed eigenfunction, respectively.

To obtain the equations of motion, define the Lagrangian as $\mathscr{L}\equiv T-V$ and substitute directly $\mathscr{L}$ into the Lagrange's equations for a conservative system [20]. This results in

$$\frac{\mathrm{d}}{\mathrm{d}t}\frac{\partial \mathscr{L}}{\partial \dot{q}_n}-\frac{\partial \mathscr{L}}{\partial q_n}=0. \tag{4}$$

Assuming the eigenvalue form:

$$q_n(t)=\bar{q}_n \mathrm{e}^{\mathrm{i}\omega t} \tag{5}$$

leads to a standard generalized eigenvalue problem:

$$\mathbf{K}_{nm}\mathbf{q}_m=\omega^2\mathbf{M}_{nm}\mathbf{q}_m. \tag{6}$$

The elements of symmetric matrices $\mathbf{M}_{nm}$ and $\mathbf{K}_{nm}$ are:

$$M_{nm} = \int_0^1 m(x) W_n(x) W_m(x)\,\mathrm{d}x, \tag{7}$$

$$K_{nm} = \int_0^1 \frac{EI(x)}{L^4} \frac{\mathrm{d}^2 W_n}{\mathrm{d}x^2} \frac{\mathrm{d}^2 W_m}{\mathrm{d}x^2}\,\mathrm{d}x. \tag{8}$$

Functions $W_n(x)$ must satisfy the global boundary conditions. In the present work $W_n(x)$ is the set of uniform beam eigenfunctions that automatically satisfies the global clamped-free boundary conditions of the beam:

$$W_n(x) = \left(\frac{\sin\,\alpha_n - \sinh\,\alpha_n}{\cos\,\alpha_n + \cosh\,\alpha_n}\right)(\sinh\,\alpha_n x - \sin\,\alpha_n x) + (\cosh\,\alpha_n x - \cos\,\alpha_n x). \tag{9}$$

For large n, the evaluation of Eq. (9) becomes numerically unstable due to the difference between large values of the hyperbolic functions. Therefore, an asymptotic approximation from Dowell [21] is used for higher modes to avoid numerical error:

$$W_n(x) = \sin\,\alpha_n x - \cos\,\alpha_n x + \mathrm{e}^{-\alpha_n x} + (-1)^{n+1}\mathrm{e}^{-\alpha_n(1-x)} + O[\varepsilon]. \tag{10}$$

The order of error is $\varepsilon = \mathrm{e}^{-\alpha_n}$, which is negligible for $n \geqslant 5$. This approach resolves the "numerical instability" issue of higher approximations using beam modes as reported by Yamada et al. [22].

The Rayleigh–Ritz method mathematically guarantees modal convergence yet requires that only the global boundary conditions be satisfied. The local geometric boundary conditions are explicitly addressed by component modal analysis in the next section.

2.2. Component modal analysis

Consider a non-uniform beam partitioned into C uniform components that are individually characterized as free–free beams. The deflection of the cth component can be written as an extension of Eq. (3):

$$w^{(c)}(\hat{x}, t) = \sum_n q_n^{(c)}(t)\chi_n(\hat{x}). \tag{11}$$

Each component is assumed to be described by the same number of basis functions. The spanwise variable $\hat{x}$ describes the non-dimensional *local* coordinate of the cth component. Each component has a spanwise length $l^{(c)}$ and flexural stiffness $(EI)^{(c)}$. The eigenfunction $\chi_n(\hat{x})$ is the nth free–free beam mode [23]:

$$\chi_n(\hat{x}) = \left(\frac{\cos\,\gamma_n - \cosh\,\gamma_n}{\sinh\,\gamma_n - \sin\,\gamma_n}\right)(\sinh\,\gamma_n\hat{x} + \sin\,\gamma_n\hat{x}) + (\cosh\,\gamma_n\hat{x} + \cos\,\gamma_n\hat{x}). \tag{12}$$

The free–free beam eigenvalue γ_n is the nth root of the following transcendental equation:

$$1 - \cos\,\gamma_n\,\cosh\,\gamma_n = 0. \tag{13}$$

The first eigenfunction is the rigid-body mode corresponding to $\gamma_1 = 0$. An asymptotic form of Eq. (12) is given by Dowell [21]:

$$\chi_n(\hat{x}) = -\sin\,\gamma_n\hat{x} + \cos\,\gamma_n\hat{x} + \mathrm{e}^{-\gamma_n\hat{x}} - (-1)^n\mathrm{e}^{-\gamma_n(1-\hat{x})} + O[\varepsilon]. \tag{14}$$

The order of error is $\varepsilon = \mathrm{e}^{-\gamma_n}$ as in Eq. (10).

The total system kinetic energy T and linear strain energy V are written as

$$T = \frac{1}{2}\sum_{c=1}^{C}\sum_n M_n^{(c)}(\dot{q}_n^{(c)}(t))^2, \tag{15}$$

$$V = \frac{1}{2}\sum_{c=1}^{C}\sum_n \left(\frac{EI}{l^3}\right)^{(c)} \gamma_n^4 (q_n^{(c)}(t))^2, \tag{16}$$

where

$$M_n^{(c)} \equiv M^{(c)} \int_0^1 (\chi_n(\hat{x}))^2 \, \mathrm{d}x. \tag{17}$$

The cross-terms seen in the Rayleigh–Ritz method do not appear here because the basis functions $\chi_n(\hat{x})$ are mutually orthogonal over each constant property component. $M^{(c)}$ is the total mass of the cth component.

To incorporate the inter-component compatibility conditions into the Lagrangian formulation, define the holonomic constraint equations for displacement and slope between components as $f_c(\hat{x}, t)$ and $g_c(\hat{x}, t)$, respectively:

$$f_c(\hat{x}, t) = w^{(c)}(\hat{x} = 1, t) - w^{(c+1)}(\hat{x} = 0, t), \tag{18}$$

$$g_c(\hat{x}, t) = w'^{(c)}(\hat{x} = 1, t) - w'^{(c+1)}(\hat{x} = 0, t). \tag{19}$$

By definition, the functions $f_c(\hat{x}, t)$ and $g_c(\hat{x}, t)$ must equal zero [20]. The root of the first component is constrained by choosing cantilever beam modes. The tip of the Cth component remains unconstrained.

The constraint equations augment the Lagrangian in the usual fashion using Lagrange multipliers [20]:

$$\mathscr{L} = T - V + \sum_{c=1}^{C-1} (\lambda_c f_c + \mu_c g_c). \tag{20}$$

Lagrange multipliers λ and μ enforce the continuity of displacement and slope between components, respectively.

Substitute the modified Lagrangian into Eq. (4) for the constrained equations of motion for each component:

$$M_n^{(1)} \ddot{q}_n^{(1)}(t) + \left(\frac{EI}{l^3}\right)^{(1)} \gamma_n^4 q_n^{(1)}(t) - \lambda_1 \chi_n(1) - \frac{\mu_1}{l^{(1)}} \chi_n'(1) = 0, \tag{21}$$

$$M_n^{(c)} \ddot{q}_n^{(c)}(t) + \left(\frac{EI}{l^3}\right)^{(c)} \gamma_n^4 q_n^{(c)}(t) - \lambda_c \chi_n(1) + \lambda_{c-1} \chi_n(0) - \frac{\mu_c}{l^{(c)}} \chi_n'(1) + \frac{\mu_{c-1}}{l^{(c)}} \chi_n'(0) = 0, \quad c = 2, \ldots, C-1, \tag{22}$$

$$M_n^{(C)} \ddot{q}_n^{(C)}(t) + \left(\frac{EI}{l^3}\right)^{(C)} \gamma_n^4 q_n^{(C)}(t) + \lambda_{C-1} \chi_n(0) + \frac{\mu_{C-1}}{l^{(C)}} \chi_n'(0) = 0. \tag{23}$$

Substitute Eq. (11) into Eqs. (18) and (19) to describe the constraints in terms of generalized coordinates:

$$\sum_n q_n^{(c)}(t) \chi_n(1) - q_n^{(c+1)}(t) \chi_n(0) = 0, \quad c = 1, \ldots, C-1, \tag{24}$$

$$\sum_n \frac{q_n^{(c)}(t)}{l^{(c)}} \chi_n'(1) - \frac{q_n^{(c+1)}(t)}{l^{(c+1)}} \chi_n'(0) = 0, \quad c = 1, \ldots, C-1. \tag{25}$$

Klein [3] eliminates the generalized coordinates to arrive at a compact eigenvalue coefficient matrix in terms of the Lagrange multipliers. The coefficient matrix elements are not of the usual form (e.g. Eqs. (7) and (8)), but the reorganization reduces the matrix dimensions to the number of Lagrange multipliers $[(2C-2)\times(2C-2)]$.

Assume the standard eigenvalue forms of $q_n^{(c)}$, λ_c, and μ_c.

$$q_n^{(c)}(t) = \bar{q}_n^{(c)} \mathrm{e}^{\mathrm{i}\omega t}, \tag{26}$$

$$\lambda_c(t) = \bar{\lambda}_c \mathrm{e}^{\mathrm{i}\omega t}, \tag{27}$$

$$\mu_c(t) = \bar{\mu}_c \mathrm{e}^{\mathrm{i}\omega t}. \tag{28}$$

Solve for the generalized coordinates as functions of Lagrange multipliers using Eqs. (21)–(23):

$$\bar{q}_n^{(1)} = -\frac{\bar{\lambda}_1 \chi_n(1) + (\bar{\mu}_1 / l^{(1)})\chi_n'(1)}{F_n^{(1)}}, \tag{29}$$

$$\bar{q}_i^{(c)} = \frac{\bar{\lambda}_{c-1}\chi_n(0) + (\bar{\mu}_{c-1}/l^{(c)})\chi_n'(0)}{F_n^{(c)}} - \frac{\bar{\lambda}_c \chi_n(1) + (\bar{\mu}_c / l^{(c)})\chi_n'(1)}{F_n^{(c)}}, \quad c = 2, \ldots, C-1, \tag{30}$$

$$\bar{q}_n^{(C)} = \frac{\bar{\lambda}_C \chi_n(1) + (\bar{\mu}_C / l^{(C)})\chi_n'(1)}{F_n^{(C)}}, \tag{31}$$

$$F_n^{(c)} \equiv \omega^2 M_n^{(c)} - \gamma_n^4 \left(\frac{EI}{l^3}\right)^{(c)}. \tag{32}$$

Substitute Eqs. (29)–(31) into the constraint equations (24) and (25) to arrive at the eigenvalue equations and characteristic equation [3]:

$$\mathbf{\Delta}(\omega) \cdot \mathbf{\Lambda} = \mathbf{0}, \tag{33}$$

$$\det[\mathbf{\Delta}(\omega)] = 0, \tag{34}$$

where $\mathbf{\Lambda}$ is the vector of Lagrange multipliers $\bar{\lambda}_c$ and $\bar{\mu}_c$. The graphical solution of Eq. (34) demonstrates that the system eigenvalues lie between the component natural frequencies [24,25].

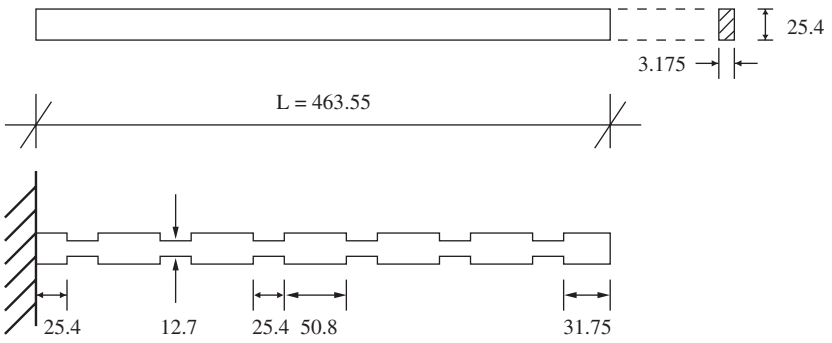

Fig. 1. Schematic of uniform and notched aluminum spar test sections (not drawn to scale). Dimensions in millimeters.

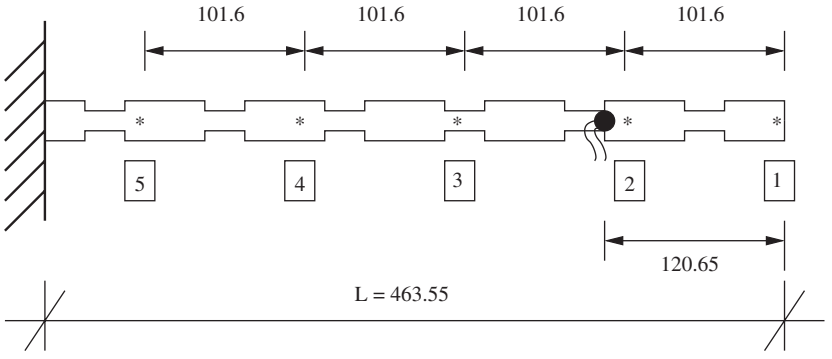

Fig. 2. Spanwise locations of impacts and accelerometer. Dimensions in millimeters.

2.3. Finite element method

All finite element calculations were performed by the commercial package ANSYS [26]. Element types BEAM4, BEAM188, SHELL93, and SOLID45 were used to model Euler–Bernoulli beam, Timoshenko beam, elastic shell, and three-dimensional elastic solid physics, respectively. The shell and solid element configurations are herein referred to as higher-dimensional models in contrast to the one-dimensional beam models.

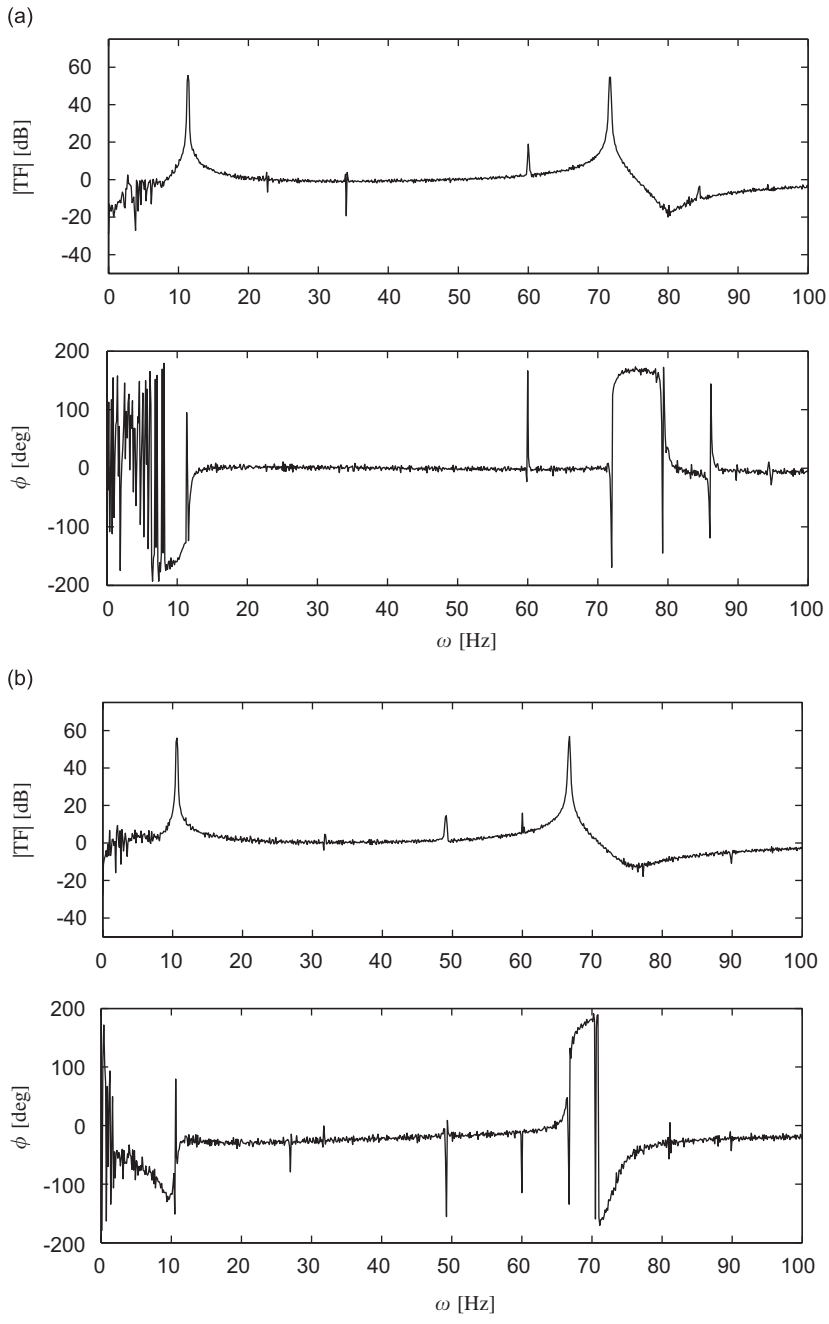

Fig. 3. Transfer functions due to flapwise impacts at the spar tip: (a) uniform spar and (b) stepped spar.

3. Experiment

The natural frequencies of a cantilevered discontinuous beam are obtained experimentally via free vibration impact testing. A uniform beam of like dimension is used as a control to determine the material properties.

Two identical aluminum spars of dimensions 635 mm × 25.4 mm × 3.175 mm are considered for this experiment. One spar is end-milled to remove 25.4 mm × 6.35 mm × 3.175 mm sections of material as shown in Fig. 1. The spar has discontinuous spanwise mass and stiffness distributions at each change in cross-sectional area.

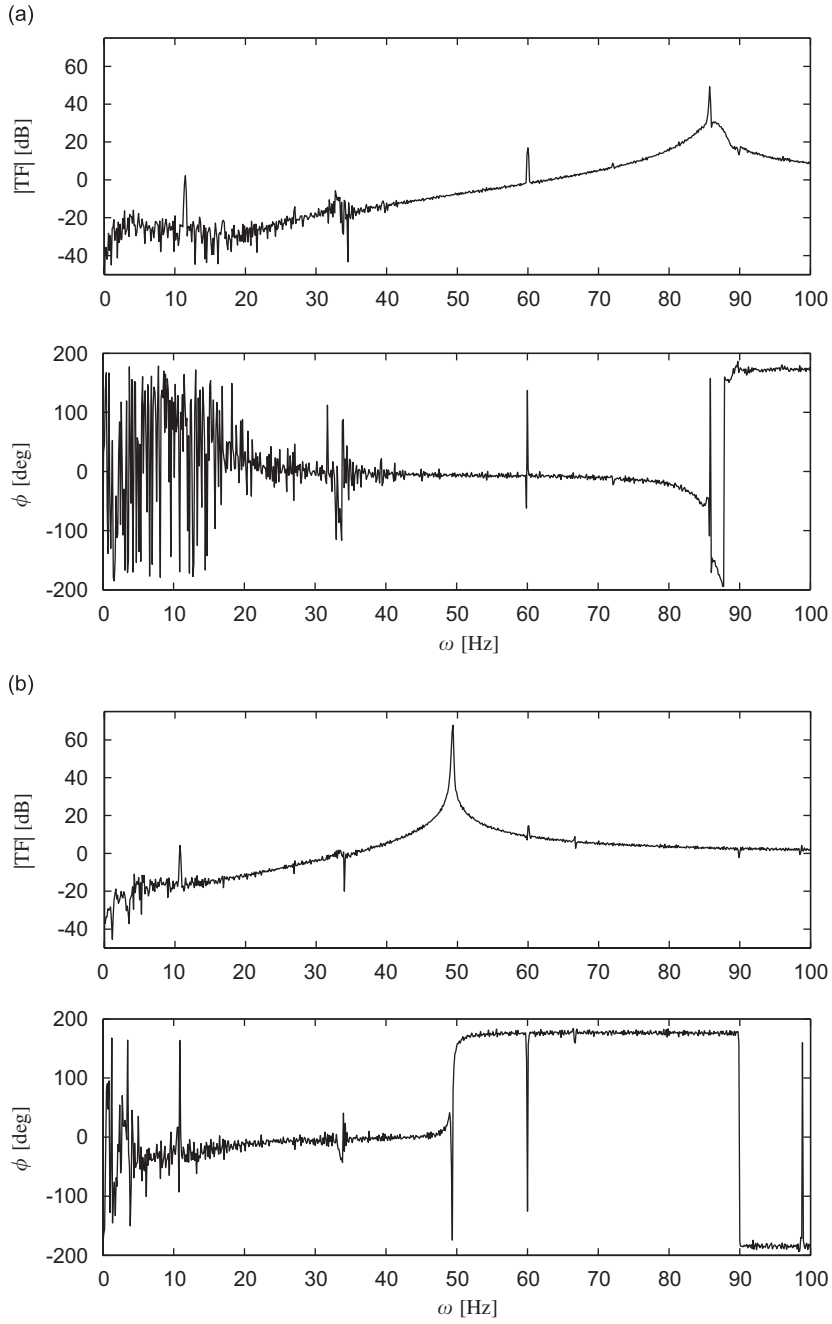

Fig. 4. Transfer functions due to chordwise impacts at the spar tip: (a) uniform spar and (b) stepped spar.

Each spar is cantilevered from a vise that is rigidly secured to a heavy table to mimic the clamped boundary condition. The spars are allowed to deflect out-of-plane (flapwise) under gravity loading. This caused some prestress from the gravitational loading, but these effects on the natural frequency results were determined to be negligible.

A transducer-fitted impact hammer (Brüel & Kjær (B&K) type 8204) is used to impart an initial velocity at the points specified in Fig. 2. An accelerometer (B&K type 4374) connected to a charge amplifier (B&K type 2635) measures the free vibration response at a fixed location. To measure the in-plane (chordwise) bending modes, the accelerometer is placed on the beam edge at the same spanwise location. The transfer function between the accelerometer and impact hammer is observed directly from a B&K PULSE data acquisition system [27], which features a built-in anti-aliasing filter. Each transfer function is averaged linearly over five hits at each impact location. Every impact is sampled at 256 Hz for 8 s to produce a frequency resolution of 125 mHz. Figs. 3 and 4 show representative transfer function results as measured from the tips of the uniform and stepped spars, respectively.

The aluminum density and elastic modulus are $\rho = 2664\,\mathrm{kg/m^3}$ and $E = 60.6\,\mathrm{GPa}$, respectively. The density is calculated from total mass and dimensional data, and the elastic modulus is calibrated to the first flapwise resonance:

$$E = \frac{12}{\alpha_1^4}\left(\frac{L}{h}\right)^2 \rho\omega_{1B}^2 L^2, \tag{35}$$

where h is the spar thickness. For a uniform Euler–Bernoulli beam, $\alpha_1 = 1.875$ [23].

The measured resonance frequencies are reported in Table 1. The first and second flapwise (out-of-plane) bending mode frequencies are denoted ω_{1B} and ω_{2B}, respectively. The first chordwise (in-plane) bending mode is identified as ω_{1C}.

4. Results and discussion

The stepped beam experimental results are compared with the theoretical and finite element values in Table 2. There is good agreement among the beam theory predictions, including the Timoshenko beam element results using ANSYS. Therefore, shear deformation and rotary inertia effects have a negligible impact on the modal results. However, there is a clear difference between the results of all the beam theories and

Table 1
Experimental natural frequencies of uniform and notched spars

Mode type	Experiment results [Hz]	
	Uniform	Notched
ω_{1B}	11.38	10.63
ω_{2B}	71.75	66.75
ω_{1C}	85.75	49.38

Table 2
Modal results comparison [Hz] for the notched spar; theoretical results are for 500 degrees-of-freedom

Mode	Rayleigh–Ritz	CMA	ANSYS				Experiment
	Euler	Euler	Euler	Timoshenko	2D Shell	3D Solid	
ω_{1B}	10.752	10.816	10.745	10.745	10.44	10.46	10.63
ω_{2B}	67.429	67.463	67.469	67.456	65.54	65.70	66.75
ω_{1C}	54.795	54.985	54.469	54.429	49.62	49.83	49.38

experiment for the first chordwise bending mode. Thus, the increase in beam model fidelity considered here does not resolve the apparent disagreement between analytical and experimental values.

It is clear from Table 2 that the beam methods used do not capture completely the physics of the higher-dimensional shell and solid element models, whose results agree well with the experimental values. This disagreement supports the hypothesis that non-beam effects are important for this configuration and are

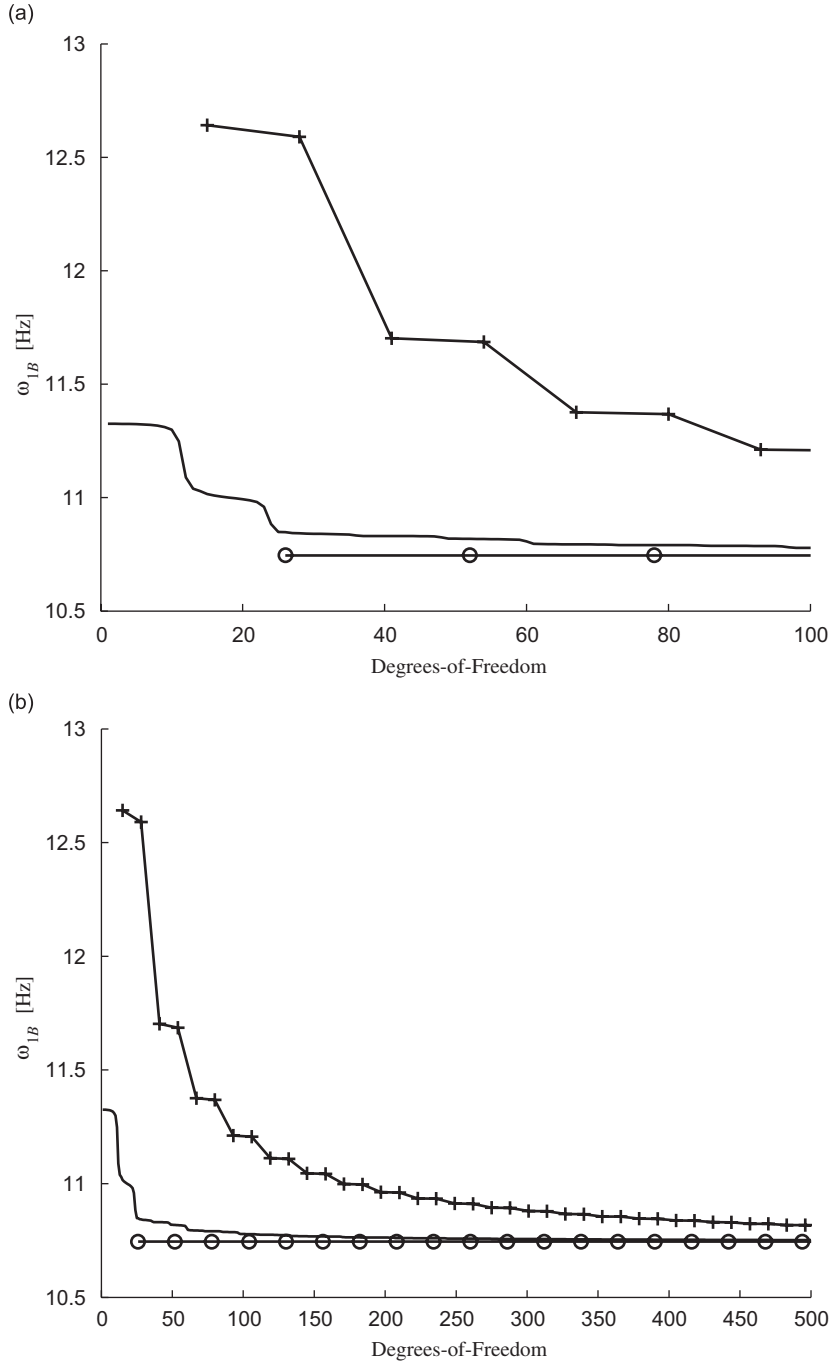

Fig. 5. Degree-of-freedom (dof) convergence of the first out-of-plane bending mode, ω_{1B}: (a) 100 dof and (b) 500 dof. –, Rayleigh–Ritz; +, component modal analysis; ○, ANSYS.

linked directly to the magnitude and geometry of the cross-section discontinuities. To the authors' knowledge, the importance of higher-dimensional effects on the modal properties of stepped beams without step eccentricity has not been previously reported in the literature. Prediction of the resonance frequencies of multiple-stepped beams without regard for non-beam effects for the present configuration results in a 10% error for the in-plane resonance.

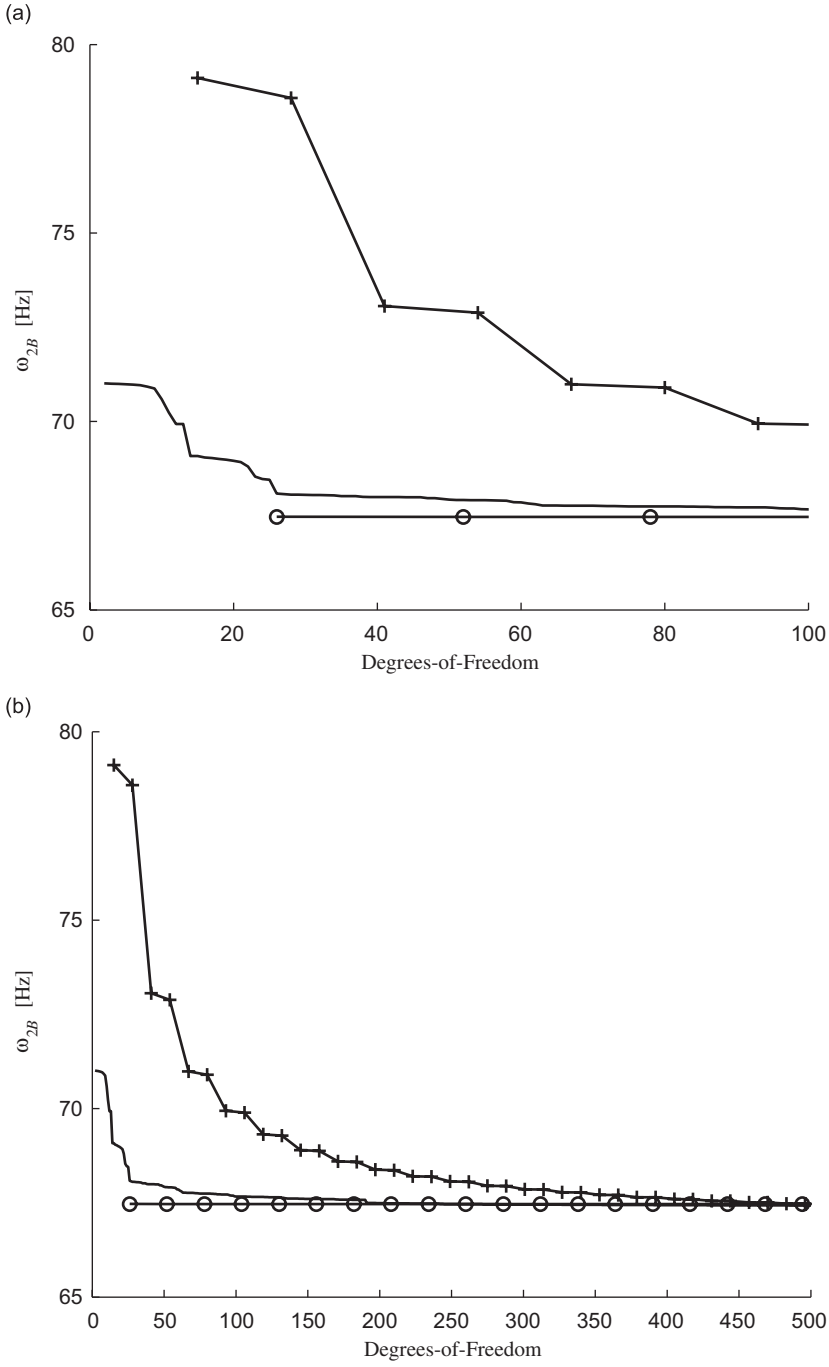

Fig. 6. Degree-of-freedom (dof) convergence of the second out-of-plane bending mode, ω_{2B}: (a) 100 dof, (b) 500 dof. –, Rayleigh–Ritz; +, component modal analysis; ○, ANSYS.

Figs. 5–7 compare the solution methods using Euler–Bernoulli theory on a degree-of-freedom (dof) basis. The finite element method converges the fastest of the three methods for all resonances. For the first in-plane mode of the presently considered notched beam configuration, the Rayleigh–Ritz method is a poor approximation for a small number of retained modes, yet converges to a more accurate eigenvalue than the component modal analysis beyond 25 dof. This result indicates that the local natural boundary conditions between components are necessary for a better low-order approximation. Also, for greater accuracy a global

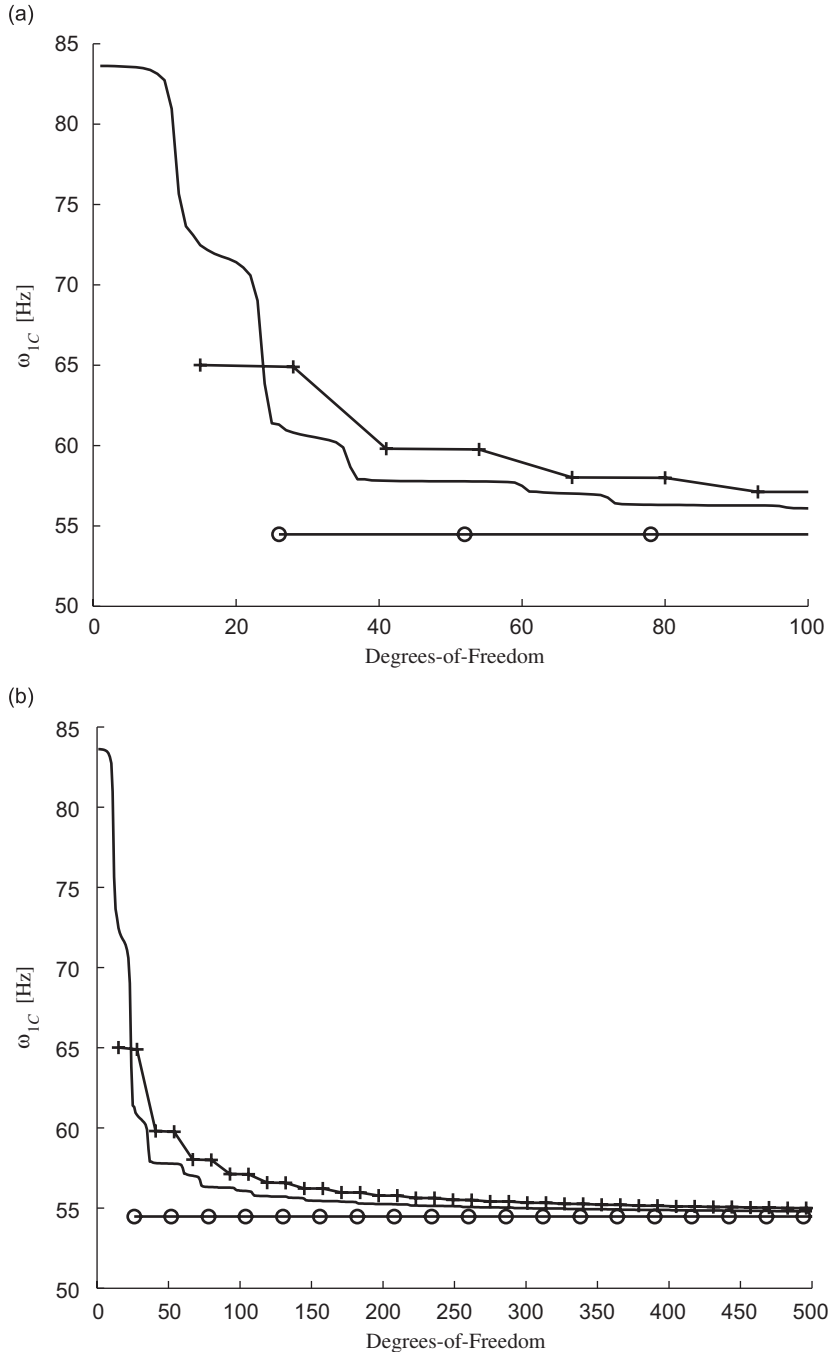

Fig. 7. Degree-of-freedom (dof) convergence of the first in-plane bending mode, ω_{1C}: (a) 100 dof, (b) 500 dof. −, Rayleigh–Ritz; +, component modal analysis; ○, ANSYS.

approach yields a better approximation and convergence of the global eigenvalue parameter. The global approach works better for the out-of-plane modes where the discontinuity is weaker.

5. Conclusion

The three lowest natural frequencies of a multiple-stepped beam are predicted using a global Rayleigh–Ritz formulation, component modal analysis, and the commerical finite element code ANSYS and are matched with experimental results from impact testing data. A comparison of the results supports the following conclusions.

The local boundary conditions between uniform property components are important for low-order vibration analyses of structures with strong discontinuities. Global methods, such as classical Rayleigh–Ritz, provide more accurate results for global parameters once either enough degrees-of-freedom are introduced or the discontinuity strength is sufficiently weak.

The disagreement between beam model and experimental results is modest, but distinct, and is attributed to non-beam effects present in the higher-dimensional elasticity models, but absent in Euler–Bernoulli and Timoshenko beam theories. This conclusion is corroborated by predictions from one-, two-, and three-dimensional finite element models.

Acknowledgment

This work was supported by Air Force Office of Scientific Research Grant FA9550-04-1-0071, "A Study of Uncertainties in Nonlinear Aeroelastic Systems," under the direction of Dr. Victor Giurgiutiu.

References

[1] N.J. Taleb, E.W. Suppiger, Vibration of stepped beams, *Journal of the Aerospace Sciences* 28 (1961) 295–298.
[2] F. Buckens, Eigenfrequencies of nonuniform beams, *AIAA Journal* 1 (1) (1963) 121–127.
[3] L. Klein, Transverse vibrations of non-uniform beams, *Journal of Sound and Vibration* 37 (4) (1974) 491–505.
[4] J. Yuan, S.M. Dickinson, On the use of artificial springs in the study of the free vibrations of systems comprised of straight and curved beams, *Journal of Sound and Vibration* 153 (2) (1992) 203–216.
[5] M.J. Maurizi, P.M. Bellés, Free vibration of stepped beams elastically restrained against translation and rotation at one end, *Journal of Sound and Vibration* 163 (1) (1993) 188–191.
[6] M.J. Maurizi, P.M. Bellés, Natural frequencies of one-span beams with stepwise variable cross-section, *Journal of Sound and Vibration* 168 (1) (1993) 184–188.
[7] H.P. Lee, T.Y. Ng, Vibration and buckling of a stepped beam, *Applied Acoustics* 42 (1994) 257–266.
[8] N. Popplewell, Daqing Chang, Free vibrations of a complex Euler–Bernoulli beam, *Journal of Sound and Vibration* 190 (5) (1996) 852–856.
[9] M. Levinson, Vibrations of stepped strings and beams, *Journal of Sound and Vibration* 49 (2) (1976) 287–291.
[10] S.K. Jang, C.W. Bert, Free vibration of stepped beams: exact and numerical solutions, *Journal of Sound and Vibration* 130 (2) (1989) 342–346.
[11] S.K. Jang, C.W. Bert, Free vibration of stepped beams: higher mode frequencies and effects of steps on frequency, *Journal of Sound and Vibration* 132 (1) (1989) 164–168.
[12] S. Naguleswaran, Natural frequencies, sensitivity and mode shape details of an Euler–Bernoulli beam with one-step change in cross-section and with ends on classical supports, *Journal of Sound and Vibration* 252 (4) (2002) 751–767.
[13] S. Naguleswaran, Vibration of an Euler–Bernoulli beam on elastic end supports with up to three step changes in cross-section, *International Journal of Mechanical Sciences* 44 (2002) 2541–2555.
[14] G. Subramanian, T.S. Balasubramanian, Beneficial effects of steps on the free vibration characteristics of beams, *Journal of Sound and Vibration* 118 (3) (1987) 555–560.
[15] P.A.A. Laura, R.E. Rossi, J.L. Pombo, D. Pasqua, Dynamic stiffening of straight beams of rectangular cross-section: a comparison of finite element predictions and experimental results, *Journal of Sound and Vibration* 150 (1) (1991) 174–178.
[16] D.J. Gorman, *Free Vibration Analysis of Beams and Shafts*, Wiley, New York, 1975.
[17] M.A. Koplow, A. Bhattacharyya, B.P. Mann, Closed form solutions for the dynamic response of Euler–Bernoulli beams with step changes in cross section, *Journal of Sound and Vibration* 295 (2006) 214–225.
[18] F. Ju, P. Lee, K.H. Lee, On the free vibrations of stepped beams, *International Journal of Solids and Structures* 31 (22) (1994) 3125–3137.

[19] S.H. Farghaly, T.H. Elmahdy, The gain in the fundamental frequency of Timoshenko beams consisting of three distinct parts and with root flexibilities, *Journal of Sound and Vibration* 178 (1) (1994) 131–140.
[20] H. Goldstein, C. Poole, J. Safko, *Classical Mechanics*, third ed., Addison-Wesley, San Francisco, CA, 2002.
[21] E.H. Dowell, On asymptotic approximations to beam model shapes, *Journal of Applied Mechanics* 51 (1984) 439.
[22] G. Yamada, Y. Kobayashi, T. Tomioka, Vibration analysis of cantilever beam systems which consist of two segments by Ritz method with various combinations of the admissible functions, *Journal of Sound and Vibration* 170 (2) (1994) 280–288.
[23] R.L. Bisplinghoff, H. Ashley, R.L. Halfman, *Aeroelasticity*, Dover Publications, Inc., New York, 1996.
[24] E.H. Dowell, On some general properties of combined dynamical systems, *Journal of Applied Mechanics* 46 (1979) 206–209.
[25] J.W. Jaworski, Ritz Analysis for Nonuniform Beam Models of High Aspect Ratio Wings, Master's Thesis, Duke University, 2006.
[26] ANSYS Release 10.0 Online Documentation, 2005.
[27] Brüel & Kjær North America, Inc., PULSE User Manual, 2005.